

Exploring neutrinos from proton decays catalyzed by GUT monopoles in the Sun

Hang Hu^a Jie Cheng^b Wan-Lei Guo^{c,1} Wei Wang^{a,d}

^aSchool of Physics, Sun Yat-Sen University, Guangzhou, 510275, China

^bNorth China Electric Power University, Beijing, 102206, China

^cInstitute of High Energy Physics, Chinese Academy of Sciences, Beijing 100049, China

^dSino-French Institute of Nuclear Engineering and Technology, Sun Yat-Sen University, Zhuhai, 519000, China

E-mail: huhang3@mail2.sysu.edu.cn, chengjie@ncepu.edu.cn, guowl@ihep.ac.cn, wangw223@mail.sysu.edu.cn

Abstract. We explore the neutrino signals from proton decays catalyzed by GUT monopoles in the Sun. Three typical proton decay modes, $p \rightarrow e^+\pi$, $p \rightarrow \mu^+K^0$ and $p \rightarrow \bar{\nu}_e\pi^+$, have been analyzed for the Super-Kamiokande experiment. The monopole-induced neutrinos arise from interactions and subsequent decays of the proton decay products. To obtain the neutrino energy spectra, we use the Geant4 software to simulate propagations of daughter particles in the highly-dense solar center. It is found that K^0 can produce a large amount of 236 MeV monoenergetic ν_μ neutrinos through the charge exchange process $K^0 + p \rightarrow K^+ + n$ and the subsequent decay $K^+ \rightarrow \mu^+\nu_\mu$ at rest. Based on this interesting feature, $p \rightarrow \mu^+K^0$ can give the best discovery potential among three decay modes for most of the parameter space. In addition, we present the Super-Kamiokande sensitivities to the monopole flux for three proton decay modes.

¹Corresponding author.

Contents

1	Introduction	1
2	Monopole-catalyzed proton decays in the Sun	2
3	Neutrino fluxes at the Earth	3
4	Neutrino detections in Super-K	5
4.1	Analysis of $p \rightarrow e^+ \pi$	6
4.2	Analysis of $p \rightarrow \mu^+ K^0$	6
4.3	Analysis of $p \rightarrow \bar{\nu}_e \pi^+$	7
5	The Super-K sensitivities	9
6	Conclusions	10

1 Introduction

The existence of magnetic monopoles is an inherent prediction of all Grand Unified Theories (GUTs), since these theories will break spontaneously down to a subgroup containing the electromagnetic U(1) factor [1, 2]. The GUT monopole mass M_M is related to the unification scale M_{GUT} , and is the order of $10^{17} - 10^{18}$ GeV for $M_{\text{GUT}} \sim 10^{16}$ GeV [3]. However, no generally convincing experimental evidence of GUT monopoles has been found [4–6]. Rubakov [7] and Callan [8] indicate that some certain GUT monopoles traversing the matter can catalyze nucleon decay reactions with a cross section of ordinary strong interactions, such as $p + \text{monopole} \rightarrow e^+ + \pi^0 + \text{monopole}$. Significant efforts have been made to directly search for nucleon decays catalyzed by GUT monopoles, such as Kamiokande [9], Soudan [10], IMB [11], Baikal [12], MACRO [13], and IceCube [14]. In addition, GUT monopoles can be captured by celestial bodies, and the following catalyzed nucleon decays can generate heat and neutrinos. The indirect limits about the monopole abundance have been derived based on the heat observations from neutron stars [15] and white dwarfs [16], and the neutrino detections from the Sun [17, 18].

Monopole-catalyzed proton decays in the Sun can produce neutrinos through the following processes [17]: $p \rightarrow e^+ \pi$, $\pi \rightarrow \pi^+$, $\pi^+ \rightarrow \mu^+ \nu_\mu$ and $\mu^+ \rightarrow e^+ \nu_e \bar{\nu}_\mu$, where the symbol π represents ρ^0, η, ω and so on. The Super-Kamiokande (Super-K) experiment has searched for these low energy neutrinos ($E_\nu \leq 53$ MeV) and given an upper limit on the monopole flux [18]. Based on the low energy SU(3)×U(1) effective theory [19], $p \rightarrow e^+ \pi$ catalyzed by the GUT monopole is the dominant neutrino production mode, namely the branching ratio $B(p \rightarrow e^+ \pi) \sim 1$. In Ref. [19], the authors predict the hierarchy of proton decay modes: $B(p \rightarrow e^+ \pi) : B(p \rightarrow \mu^+ K^0) \approx 1 : (m_d/m_s)^2$, where $(m_d/m_s)^2 \sim 1/400$ is from the short-distance current algebra masses or $(m_d/m_s)^2 \sim 1/2$ is from the long-distance constituent masses. Meanwhile, $p \rightarrow \bar{\nu}_e \pi^+$ and $p \rightarrow \mu^+ \pi$ are apparently forbidden [19]. In fact, the SU(3)×U(1) theory may allow $p \rightarrow \bar{\nu}_e \pi^+$ at a sufficiently short distance limit [20]. In this case, $p \rightarrow \bar{\nu}_e \pi^+$ has a branching ratio of $B(p \rightarrow \bar{\nu}_e \pi^+) \sim 10^{-4}$ and directly produces a monoenergetic $\bar{\nu}_e$ of 459 MeV. It is found that $p \rightarrow \bar{\nu}_e \pi^+$ can give the greater discovery potential than $p \rightarrow \mu^+ K^0$ due to the smaller background and the larger neutrino cross section [20].

In this paper, we find that K^0 from $p \rightarrow \mu^+ K^0$ can also generate the high energy neutrino (236 MeV ν_μ) through the charge exchange process $K^0 + p \rightarrow K^+ + n$ and the subsequent decay $K^+ \rightarrow \mu^+ \nu_\mu$ at rest. Compared with the K^0 decay, $K^0 + p \rightarrow K^+ + n$ is non-negligible because of the considerable proton density at the center of the Sun. Here we shall explore the Super-K discovery potentials of $p \rightarrow e^+ \pi$, $p \rightarrow \mu^+ K^0$ and $p \rightarrow \bar{\nu}_e \pi^+$ catalyzed by GUT monopoles in the Sun. This paper is organized as follows. Section 2 briefly introduce the monopole-catalyzed proton decays in the Sun. Then we discuss the neutrino production from three typical proton decay modes in section 3, and give the corresponding neutrino fluxes at the Earth based on the Geant4 simulation. Section 4 shows the expected signal and background distributions in Super-K. In section 5, we calculate the Super-K sensitivities to three typical proton decay modes and compare their discovery potentials. Finally, a conclusion will be given in section 6.

2 Monopole-catalyzed proton decays in the Sun

GUT monopoles can be produced in the very early Universe as stable topological defects during phase transitions via the Kibble mechanism [21]. As the Universe expanded and cooled down, GUT monopoles could reach a speed of $\beta \sim 10^{-10}$. After the galaxy formation, they can be bound to our galaxy and be accelerated by the galactic magnetic field to $\beta \sim 10^{-3} \sqrt{10^{17} \text{ GeV} / M_M}$ for the monopole mass $M_M \gtrsim 10^{11} \text{ GeV}$ [3]. Comparing the energy loss rate with the regeneration rate of the galactic magnetic field, Parker obtained a bound on the monopole flux [22, 23]:

$$F_M < \begin{cases} 10^{-15} \text{ cm}^{-2} \text{ sr}^{-1} \text{ s}^{-1}, & M_M \lesssim 10^{17} \text{ GeV}, \\ 10^{-15} \left(\frac{M_M}{10^{17} \text{ GeV}} \right) \text{ cm}^{-2} \text{ sr}^{-1} \text{ s}^{-1}, & M_M \gtrsim 10^{17} \text{ GeV}. \end{cases} \quad (2.1)$$

The intergalactic GUT monopoles are isotropic due to the acceleration process.

Some GUT monopoles passing through the Sun can lose enough energy and are captured by the Sun. The dominant energy loss mechanism comes from the electronic interactions between GUT monopoles and electrons in the Sun [24]. The total number of monopoles trapped by the Sun is given by [17, 18]

$$\begin{aligned} N_M &= 4\pi F_M \pi R_\odot^2 \left[1 + \frac{\beta_{\text{esc}}^2}{\beta^2} \right] \epsilon(M_M, \beta, g) t_\odot \\ &= 2.8 \times 10^{25} \frac{F_M}{10^{-15} \text{ cm}^{-2} \text{ sr}^{-1} \text{ s}^{-1}} \left[1 + \frac{\beta_{\text{esc}}^2}{\beta^2} \right] \epsilon(M_M, \beta, g), \end{aligned} \quad (2.2)$$

where the solar radius $R_\odot = 7.0 \times 10^{10} \text{ cm}$ and the solar age $t_\odot = 4.6 \times 10^9 \text{ yr}$. The term in the bracket accounts for the focusing effect of the solar gravitational field, and $\beta_{\text{esc}} = 2 \times 10^{-3}$ is the escape velocity at the Sun surface. $\epsilon(M_M, \beta, g)$ describes the capture fraction of all monopoles that enter the Sun can be captured. It can be derived from the monopole stopping power [24, 25], which depends on the monopole mass M_M , velocity β and magnetic charge g . The capture fraction $\epsilon(M_M, \beta, g)$ will increase and approach 1 as the monopole mass and velocity decrease. In Refs. [24, 26], $\epsilon(M_M, \beta, g)$ has been numerically calculated by solving the monopole motion equation. For a typical GUT monopole with $M_M = 10^{16} \text{ GeV}$, $\beta = 10^{-3}$ and the Dirac magnetic charge, we can obtain $\epsilon = 0.48$ from Ref. [26] and give $N_M = 6.7 \times 10^{25}$ when F_M takes the Parker bound $1 \times 10^{-15} \text{ cm}^{-2} \text{ sr}^{-1} \text{ s}^{-1}$.

Once these GUT monopoles stop in the Sun, they will quickly fall to the solar center, and their distribution depends on the support mechanism against gravity [24]. When monopoles are supported by their own thermal pressure, the distribution radius is order of 10^2 cm. In this case, the monopole-antimonopole annihilation can drastically reduce the number of captured monopoles. If the solar center has a magnetic field of several hundred Gauss, it can support monopoles to a distance of $\sim 10^7$ cm, and prevent the annihilation [24]. In the following analysis, we assume that the trapped monopoles are uniformly distributed in the solar core of radius $r_M \sim 10^7$ cm and the monopole-antimonopole annihilation is negligible.

According to the Rubakov-Callen effect [7, 8], the captured monopoles can catalyze proton decays in the Sun. The cross section σ_R of the catalysis process behaves as [7, 8, 27]

$$\sigma_R = \frac{\sigma_0}{\beta_{\text{rel}}} \cdot F(\beta_{\text{rel}}), \quad (2.3)$$

where σ_0 is estimated to be the order of the hadronic cross sections. The relative velocity between monopoles and protons in the Sun may be taken from the Hydrogen thermal velocity, $\beta_{\text{rel}} = \sqrt{2T_\odot/m_p} = 1.7 \times 10^{-3}$ with the solar central temperature $T_\odot = 1.544 \times 10^7$ K [28]. $F(\beta_{\text{rel}})$ is a correction factor of the catalysis process for slowly moving monopoles in the matter. Based on $F(\beta_{\text{rel}})$ listed in Table I of Ref. [27], the Hydrogen element with $F(\beta_{\text{rel}}) = 0.17/\beta_{\text{rel}}$ gives a dominant contribution to monopole-catalyzed proton decays in the Sun, and contributions from other elements are negligible. The monopole-catalyzed proton decay rate in the Sun is given by [29]

$$f_p = \frac{\rho_H}{m_p} \beta_{\text{rel}} \sigma_R N_M = 9.8 \times 10^{10} \frac{\sigma_0}{1 \text{ mb}} N_M \text{ s}^{-1}, \quad (2.4)$$

where a fixed Hydrogen mass density $\rho_H = 53.9 \text{ g cm}^{-3}$ [28] has been used since these trapped monopoles are confined to a very small region $r_M/R_\odot < 0.001$.

3 Neutrino fluxes at the Earth

Monopole-catalyzed proton decays in the Sun can produce neutrinos through subsequent decays of daughter particles. On the other hand, we should consider interactions of final state mesons in the Sun, such as the π^+ absorption and the K^0 charge exchange process, which can significantly change the produced neutrino fluxes and energy spectra. In addition, these monopole-induced neutrinos will undergo the neutrino oscillation from the solar center to neutrino detectors. The neutrino flux at the surface of the Earth can be written as

$$\frac{d\Phi_{\nu_\alpha}}{dE_\nu} = \frac{f_p}{4\pi R^2} B \sum_{l=(e,\mu)} Y_{\nu_l} f_{\nu_l}(E_\nu) P_{\nu_l \rightarrow \nu_\alpha}, \quad (3.1)$$

where $\nu_\alpha = (\nu_e, \nu_\mu, \nu_\tau)$ and $R = 1.5 \times 10^{13}$ cm is the Earth-Sun distance. For the branching ratios B of three typical proton decay modes, we take

$$\begin{aligned} B(p \rightarrow e^+ \pi \rightarrow \pi^+) &\equiv B(p \rightarrow e^+ \pi) f_{\pi^+} \approx 0.5, \\ B(p \rightarrow \mu^+ K^0) &\approx m_d^2/m_s^2 \sim 1/400 - 1/2, \\ B(p \rightarrow \bar{\nu}_e \pi^+) &\approx m_p^2/m_W^2 \sim 10^{-4}, \end{aligned} \quad (3.2)$$

where $B(p \rightarrow \mu^+ K^0)$ and $B(p \rightarrow \bar{\nu}_e \pi^+)$ come from the theoretical predictions [19, 20], and $B(p \rightarrow e^+ \pi \rightarrow \pi^+)$ is the same with the Super-K assumption [18]. Note that the effective

Table 1. Neutrino yields Y_{ν_l} of three proton decay modes in the solar center from the Geant4 simulation. For the monoenergetic spectrum, the value in the parenthesis means the neutrino energy.

Decay mode	Continuous Spectrum				Monoenergetic Spectrum		
	Y_{ν_e}	$Y_{\bar{\nu}_e}$	Y_{ν_μ}	$Y_{\bar{\nu}_\mu}$	$Y_{\nu_\mu}(30)$	$Y_{\nu_\mu}(236)$	$Y_{\bar{\nu}_e}(459)$
$p \rightarrow e^+ \pi \rightarrow \pi^+$	0.89	-	-	0.89	0.89	-	-
$p \rightarrow \mu^+ K^0$	1.76	<0.01	0.01	1.74	0.55	0.18	-
$p \rightarrow \bar{\nu}_e \pi^+$	0.78	-	-	0.78	0.78	-	1.0

branching ratio $B(p \rightarrow e^+ \pi \rightarrow \pi^+)$ is defined as $B(p \rightarrow e^+ \pi)$ multiplied by the average π^+ production rate f_{π^+} from a proton decay of $p \rightarrow e^+ \pi$. In Eq. (3.1), $P_{\nu_l \rightarrow \nu_\alpha}$ is the oscillation probability of ν_l from the Sun center to ν_α at the Earth surface. In the following analysis, $P_{\nu_l \rightarrow \nu_\alpha}$ will be taken from Fig. 6 of Ref. [30], where $\theta_{13} = 8.8^\circ$ differs slightly from the current best-fit value [3]. Assuming the normal hierarchy, we get $P_{\nu_\mu \rightarrow \nu_e}(236 \text{ MeV}) = 0.48$, $P_{\bar{\nu}_e \rightarrow \bar{\nu}_\mu}(459 \text{ MeV}) = 0.67(0.23)$. In the low energy range, the oscillation probability of $P_{\bar{\nu}_\mu \rightarrow \bar{\nu}_e}$ is insensitive to the neutrino energy. It is convenient for us to take a fixed $P_{\bar{\nu}_\mu \rightarrow \bar{\nu}_e} = 0.17$ for $20 \text{ MeV} \leq E_\nu \leq 53 \text{ MeV}$.

In Eq. (3.1), Y_{ν_l} and $f_{\nu_l}(E_\nu)$ describe the ν_l yield and the normalized energy spectrum from proton decays in the Sun, respectively. In order to determine Y_{ν_l} and $f_{\nu_l}(E_\nu)$ for three typical proton decay modes, we use the Geant4 [31] software to simulate propagations of daughter particles π^+ , μ^+ and K^0 with corresponding momenta in the core of the Sun. In this simulation, the solar central density $\rho = 148.9 \text{ g/cm}^3$ and the composition of dominant elements from the AGSS09 solar model have been used [28]. The neutrino production yields are listed in Table 1. Due to inelastic reactions with nucleons, about 22% π^+ with a momentum of 459 MeV can not produce low energy neutrinos ($E_\nu \leq 53 \text{ MeV}$). As the π^+ momentum goes down to 100 MeV, Y_{ν_l} will increase from 0.78 to 0.99. Since the π^+ momentum distribution is model-dependent, we here take the average value 0.89 of 0.78 and 0.99 for $p \rightarrow e^+ \pi \rightarrow \pi^+$. K^0 can also produce low energy neutrinos through $K_S^0 \rightarrow \pi^+ \pi^-$ and the K_S^0 regeneration from K_L^0 . In addition, high energy neutrinos ($E_\nu \geq 200 \text{ MeV}$) can be expected from the direct decay of $K_L^0 \rightarrow \pi^\pm e^\mp \bar{\nu}_e / \nu_e$. The corresponding probability is estimated to be about 2.0×10^{-6} [29]. Therefore, one usually believes that high energy neutrinos are negligible for the decay mode $p \rightarrow \mu^+ K^0$. However, we find that a K^0 with a momentum of 326 MeV can averagely produce 0.18 monoenergetic 236 MeV ν_μ , $Y_{\nu_\mu}(236) = 0.18$. This is because that the charge exchange process $K^0 + p \rightarrow K^+ + n$ is no longer negligible compared with the K_S^0 decay in the highly-dense center of the Sun. Then the monoenergetic ν_μ arises from the subsequent decay of $K^+ \rightarrow \mu^+ \nu_\mu$ at rest. To test this result, We have also used the FLUKA [32] software to simulate K^0 in the solar center and obtained $Y_{\nu_\mu}(236) = 0.23$, which means that this very interesting result from the Geant4 simulation is reliable.

In Fig. 1, we plot the ν_l energy spectra $Y_{\nu_l} f_{\nu_l}(E_\nu)$ from the Geant4 simulations of $p \rightarrow \bar{\nu}_e \pi^+$ and $p \rightarrow \mu^+ K^0$ in the Sun. For the decay mode $p \rightarrow \bar{\nu}_e \pi^+$, low energy ν_μ (30 MeV), ν_e and $\bar{\nu}_\mu$ neutrinos are produced through the two-step decay process: $\pi^+ \rightarrow \mu^+ \nu_\mu$ and $\mu^+ \rightarrow e^+ \nu_e \bar{\nu}_\mu$. The obtained ν_e and $\bar{\nu}_\mu$ energy spectra are well consistent with the theoretical calculation of the μ^+ decay at rest [33]. $f_{\nu_\mu}(E_\nu) \simeq \delta(E_\nu - 30 \text{ MeV})$ implies that the π^+ decaying in the flight is negligible due to the large density in the solar center. For $p \rightarrow e^+ \pi$, $f_{\nu_l}(E_\nu \leq 53 \text{ MeV})$ from $p \rightarrow \bar{\nu}_e \pi^+$ will be used. For the decay mode $p \rightarrow \mu^+ K^0$, low energy neutrinos ν_e and $\bar{\nu}_\mu$ have three dominant sources: the final state μ^+ , π^+ in $K_S^0 \rightarrow \pi^+ \pi^-$ and

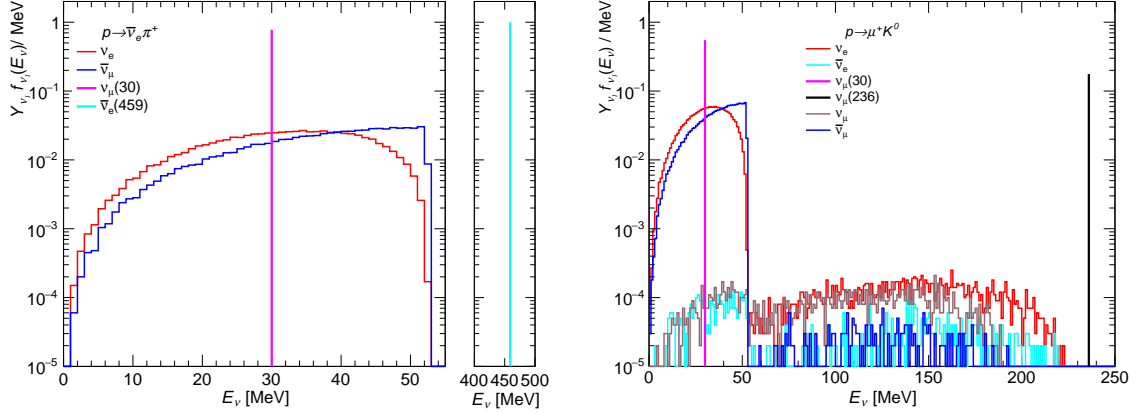


Figure 1. The neutrino energy spectra $Y_{\nu_i} f_{\nu_i}(E_{\nu})$ evaluated by the Geant4 simulation for monopole-catalyzed proton decays $p \rightarrow \bar{\nu}_e \pi^+$ (left) and $p \rightarrow \mu^+ K^0$ (right) in the Sun.

μ^+ in $K^+ \rightarrow \mu^+ \nu_\mu$. On the other hand, the continuous spectrum of the low energy ν_μ comes from μ^- and ν_μ in $K_L^0 \rightarrow \pi^\pm \mu^\mp \bar{\nu}_\mu / \nu_\mu$, and ν_μ in $K^+ \rightarrow \pi^0 \mu^+ \nu_\mu$. It is clear that the μ^- decay leads to a significant change for the ν_μ continuous spectrum at 53 MeV. As shown in the right panel of Fig. 1, K^0 can produce a small amount of ν_e , $\bar{\nu}_e$, ν_μ and $\bar{\nu}_\mu$ in the energy range of $53 \text{ MeV} \leq E_\nu \leq 230 \text{ MeV}$. We find that the antineutrino spectra are far smaller than the neutrino spectra in this region. It means that these neutrinos mainly arise from the K^+ decay processes $K^+ \rightarrow \pi^0 e^+ \nu_e$ and $K^+ \rightarrow \pi^0 \mu^+ \nu_\mu$, rather than from $K_L^0 \rightarrow \pi^\pm e^\mp \bar{\nu}_e / \nu_e$ and $K_L^0 \rightarrow \pi^\pm \mu^\mp \bar{\nu}_\mu / \nu_\mu$. Because of $Y_{\nu_i} \sim 1\%$ in this range, we do not consider their contributions in the following analysis.

4 Neutrino detections in Super-K

Here we shall discuss the neutrino signals in the Super-K detector from monopole-catalyzed proton decays. The expected ν_α event number from the charged current (CC) interaction can be calculated by

$$N_{\nu_\alpha} = N_{\text{target}} T \int \frac{d\Phi_{\nu_\alpha}}{dE_\nu} \sigma_{\nu_\alpha}(E_\nu) dE_\nu, \quad (4.1)$$

where N_{target} is the target number and the exposure time $T = 7.8$ years will be taken for the comparison with the previous result in Ref. [18]. One can quickly obtain 1.5×10^{33} free protons and 7.5×10^{32} water molecules from the Super-K fiducial mass of 22.5 ktons. Here we only consider the inverse beta decay (IBD) reaction for the decay mode $p \rightarrow e^+ \pi$ since its event rate is far larger than the electron elastic scattering [18]. The IBD cross section $\sigma_{\bar{\nu}_e}(E_\nu)$ can be found in Ref. [34], which is the order of $10^{-41} - 10^{-40} \text{ cm}^2$ in the energy range of $20 \text{ MeV} \leq E_\nu \leq 53 \text{ MeV}$. For high energy neutrinos, we evaluate the CC cross sections per water molecule from the GENIE database [35], and obtain $\sigma_{\nu_e}(236 \text{ MeV}) = 2.51 \times 10^{-38} \text{ cm}^2$, $\sigma_{\bar{\nu}_e}(459 \text{ MeV}) = 2.16 \times 10^{-38} \text{ cm}^2$ and $\sigma_{\bar{\nu}_\mu}(459 \text{ MeV}) = 2.00 \times 10^{-38} \text{ cm}^2$. It is clear that they are much larger than the low energy IBD cross section. So only the high energy neutrino events will be analyzed for the proton decay modes $p \rightarrow \bar{\nu}_e \pi^+$ and $p \rightarrow \mu^+ K^0$ in the following parts. With the help of Eqs. (3.1) and (4.1), we can express the expected ν_α event number

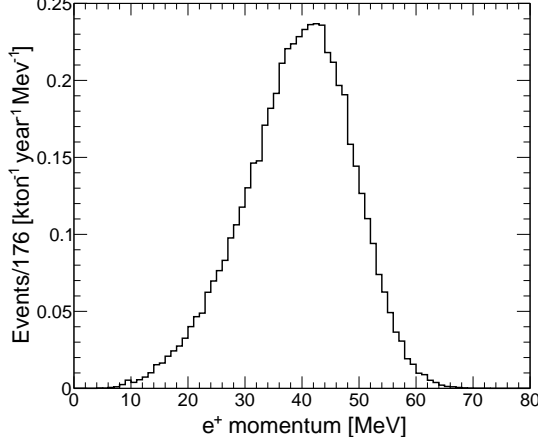


Figure 2. The expected distribution of the IBD events as a function of the e^+ momentum with $f_p/(4\pi R^2)B(p \rightarrow e^+\pi \rightarrow \pi^+) = 1 \text{ cm}^{-2}\text{s}^{-1}$ and the Super-K 176 kton-year exposure.

as

$$\begin{aligned}
 N_{\bar{\nu}_e}(\leq 53 \text{ MeV}) &= 5.49 \times \frac{f_p/(4\pi R^2)}{1 \text{ cm}^{-2} \text{ s}^{-1}} \times B(p \rightarrow e^+\pi \rightarrow \pi^+), \\
 N_{\nu_e}(236 \text{ MeV}) &= 3.94 \times 10^2 \times \frac{f_p/(4\pi R^2)}{1 \text{ cm}^{-2} \text{ s}^{-1}} \times B(p \rightarrow \mu^+ K^0), \\
 N_{\bar{\nu}_e}(459 \text{ MeV}) &= 2.68 \times 10^3 \times \frac{f_p/(4\pi R^2)}{1 \text{ cm}^{-2} \text{ s}^{-1}} \times B(p \rightarrow \bar{\nu}_e \pi^+), \\
 N_{\bar{\nu}_\mu}(459 \text{ MeV}) &= 8.52 \times 10^2 \times \frac{f_p/(4\pi R^2)}{1 \text{ cm}^{-2} \text{ s}^{-1}} \times B(p \rightarrow \bar{\nu}_e \pi^+),
 \end{aligned} \tag{4.2}$$

for the 176 kton-year exposure of the Super-K detector.

4.1 Analysis of $p \rightarrow e^+\pi$

The Super-K experiment has performed the search of monopole-induced neutrinos from the decay mode $p \rightarrow e^+\pi$ [18]. In order to compare the significances of three proton decay modes, we here do not cite the Super-K result, and shall adopt an uniform method to estimate their sensitivities. The expected distribution of IBD events as a function of the e^+ momentum p_e is shown in Fig. 2. Note that the momentum resolution of $0.6 + 2.6/\sqrt{p_e(\text{GeV})}\%$ [36] has been included in this figure. To reduce backgrounds from the spallation products and solar neutrinos, we take the momentum cut $20 \text{ MeV} \leq p_e \leq 55 \text{ MeV}$, which is basically consistent with the selection condition [19-55] MeV on the reconstructed event energy [18]. Considering the above momentum range and other cuts listed in Table 1 of Ref. [18], we may derive the signal efficiency $\varepsilon = 0.82$. In this case, the expected background number $N_{\text{bkg}} \simeq 300$ and the observed event number $N_{\text{obs}} = 317$ can be found in Ref. [18]. The background events are dominantly caused by atmospheric neutrino interactions, such as the decay electrons from invisible muons, the final state electrons and the multiple de-excitation γ -rays from residual nuclei.

4.2 Analysis of $p \rightarrow \mu^+ K^0$

For the 236 MeV ν_μ produced by $p \rightarrow \mu^+ K^0$ in the Sun, the Super-K experiment can observe ν_μ and ν_e CC events due to the neutrino oscillation possibility $P_{\nu_\mu \rightarrow \nu_e}(236\text{MeV}) = 0.48$. We

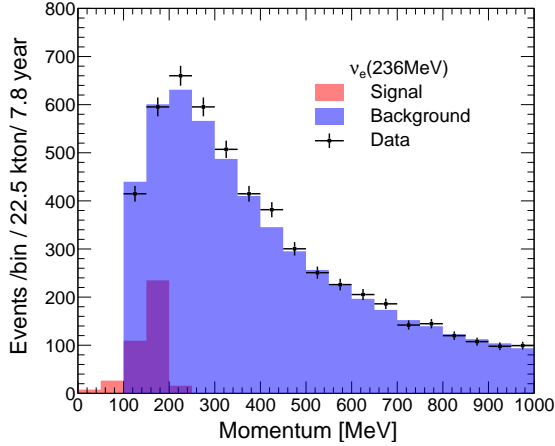


Figure 3. The expected momentum distribution of electrons from the 236 MeV ν_e CC interaction assuming $f_p/(4\pi R^2)B(p \rightarrow \mu^+ K^0) = 1 \text{ cm}^{-2}\text{s}^{-1}$. The background and observed momentum distributions come from Ref. [37], and are scaled to the level of 176 kton-year exposure.

use the GENIE generator to simulate the ν_μ and ν_e CC interactions in the water. It is found that the average momentum of the final state μ^- is about 127 MeV. In this case, the Super-K can not effectively use the 236 MeV ν_μ CC events. So we only calculate the ν_e contribution for the $p \rightarrow \mu^+ K^0$ analysis. The momentum distribution of electrons from the 236 MeV ν_e CC interaction is shown in Fig. 3, where a momentum resolution of $0.6 + 2.6/\sqrt{p_e(\text{GeV})}\%$ has been used. It is clear that most events give $p_e \geq 100$ MeV. The momentum distributions of background and observed events in the Super-K detector have also been plotted in Fig. 3. These data come from Ref. [37], and are scaled to the level of 176 kton-year exposure. Comparing the signal and background distributions, we set the selection condition $100 \text{ MeV} \leq p_e \leq 200 \text{ MeV}$ to reduce atmospheric neutrino backgrounds and increase the discovery potential of $p \rightarrow \mu^+ K^0$. The corresponding signal efficiency ε , background number N_{bkg} and observed number N_{obs} have been summarized in Table 2. Here we do not consider the direction cut about the final state electrons since their directions from the GENIE simulation are nearly isotropic at this energy.

4.3 Analysis of $p \rightarrow \bar{\nu}_e \pi^+$

For the 459 MeV $\bar{\nu}_e$ from $p \rightarrow \bar{\nu}_e \pi^+$, we shall analyze both $\bar{\nu}_e$ and $\bar{\nu}_\mu$ CC events in the Super-K detector due to large neutrino oscillation probabilities $P_{\bar{\nu}_e - \bar{\nu}_\mu}(459 \text{ MeV}) = 0.67(0.23)$. For single-ring e -like (μ -like) events in Super-K, the momentum and angular resolutions are estimated to be $0.6 + 2.6/\sqrt{p_l(\text{GeV})}\%$ ($1.7 + 0.7/\sqrt{p_l(\text{GeV})}\%$) and 3.0° (1.8°) [36], respectively. Based on the GENIE simulations of the 459 MeV $\bar{\nu}_e$ and $\bar{\nu}_\mu$ CC interactions, one can determine the momentum and angular distributions of the final state particles e^+ and μ^+ as shown in Fig. 4. θ is defined as the angle between the initial neutrino direction (the Sun direction) and the charged lepton direction. Unlike the 236 MeV ν_e CC interaction, the 459 MeV $\bar{\nu}_e$ and $\bar{\nu}_\mu$ CC events show the directional feature. This is because that antineutrinos will statistically transfer more momentum to the charged lepton than neutrinos in the CC interactions. In Fig. 4, the momentum distributions of atmospheric neutrino backgrounds and observed data in Super-K come from Ref. [37], and are scaled to the level of 176 kton-year exposure. Assuming they have a uniform angular distribution, we scan the parameter space

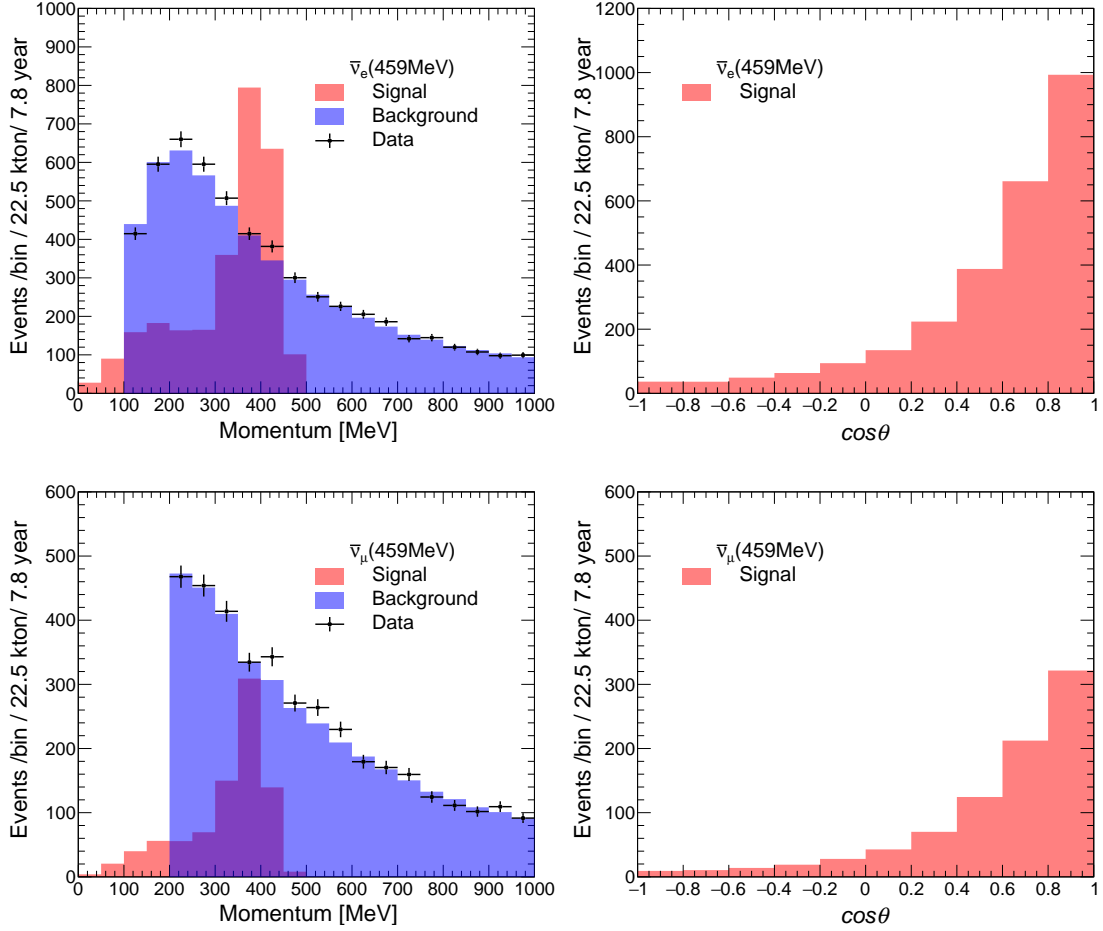


Figure 4. The expected momentum (left) and angular (right) distributions of charged leptons from the 459 MeV $\bar{\nu}_e$ (upper panels) and $\bar{\nu}_\mu$ (lower panels) CC interactions assuming $f_p/(4\pi R^2)B(p \rightarrow \bar{\nu}_e \pi^+) = 1 \text{ cm}^{-2}\text{s}^{-1}$. The background and observed momentum distributions come from Ref. [37], and are scaled to the level of 176 kton-year exposure.

Table 2. Summary of the analyzed neutrinos, the corresponding selection criteria on momentum p_l and angle $\cos \theta$, background number N_{bkg} , observed number N_{obs} , signal efficiency ε , and 90% C.L. upper limit N_{90} on the expected signal number in Super-K for three proton decay modes.

Decay mode	Neutrino	p_l (MeV)	$\cos \theta$	N_{bkg}	N_{obs}	ε	N_{90}
$p \rightarrow e^+ \pi^- \rightarrow \pi^+$	$\bar{\nu}_e (\leq 53)$	[20, 55]	-	300	317	0.82	42.85
$p \rightarrow \mu^+ K^0$	$\nu_e (236)$	[100, 200]	-	1040.6	1010.1	0.87	38.58
$p \rightarrow \bar{\nu}_e \pi^+$	$\bar{\nu}_e (459)$	[350, 450]	≥ 0.6	151.1	159.3	0.33	32.65
	$\bar{\nu}_\mu (459)$	[350, 400]	≥ 0.4	100.3	100.4	0.28	

of the charged lepton momentum p_l and direction $\cos \theta$ to maximize the Super-K discovery potential. The optimal selection criteria on p_l and $\cos \theta$, and the corresponding signal efficiency ε , background number N_{bkg} and observed number N_{obs} , have been listed in Table 2.

5 The Super-K sensitivities

To estimate the Super-K sensitivities to three typical proton decay modes, we firstly calculate the 90% confidence level (C.L.) upper limit N_{90} on the expected signal number N_s through the following formulas [38, 39]

$$90\% = \frac{\int_{N_s=0}^{N_{90}} L(N_{\text{obs}}|N_s) dN_s}{\int_{N_s=0}^{\infty} L(N_{\text{obs}}|N_s) dN_s}, \quad (5.1)$$

with the Poisson-based likelihood function

$$L(N_{\text{obs}}|N_s) = \prod_{i=1}^2 \frac{(N_s F^i + N_{\text{bkg}}^i)^{N_{\text{obs}}^i}}{N_{\text{obs}}^i!} e^{-(N_s F^i + N_{\text{bkg}}^i)}, \quad (5.2)$$

where the index i refers to the classification of expected signals. F^i denotes the fraction of each category, and can be determined from $N_{\nu_\alpha}^i$ in Eq. (4.2) and the corresponding ε^i in Table 2. For $p \rightarrow \bar{\nu}_e \pi^+$, two fractions of $F^1 = 0.79$ and $F^2 = 0.21$ refer to the 459 MeV $\bar{\nu}_e$ and $\bar{\nu}_\mu$ categories, respectively. For the other two decay modes, we only analyze a type of signal and take $F^1 = 1$. With the help of the background number N_B^i and observed number N_{obs}^i , the corresponding N_{90} of each decay mode has been calculated and listed in the last column of Table 2.

Then we use the formula

$$N_{90} = \sum_{i=1}^2 N_{\nu_\alpha}^i \varepsilon^i \quad (5.3)$$

to estimate the 90% C.L. upper limit to the monopole-catalyzed proton decay rate f_p in the Sun. In the left panel of Fig. 5, we plot the Super-K upper limits on f_p for three typical proton decay modes, where the branching ratios $B(p \rightarrow e^+ \pi \rightarrow \pi^+) = 0.5$, $B(p \rightarrow \mu^+ K^0) = (m_d/m_s)^2 \sim 1/400 - 1/2$ and $B(p \rightarrow \bar{\nu}_e \pi^+) = 10^{-4}$ have been used. It is clear that the decay mode $p \rightarrow \mu^+ K^0$ always give a better limit than $p \rightarrow \bar{\nu}_e \pi^+$. For $B(p \rightarrow \mu^+ K^0) = (m_d/m_s)^2 > 6.0 \times 10^{-3}$, the best experimental limit will come from $p \rightarrow \mu^+ K^0$ among all three proton decay modes. So we suggest the Super-K collaboration searches for this important proton decay mode in the future analysis.

Finally, we calculate the Super-K upper limit on the monopole flux by use of Eqs. (2.2) and (2.4) as shown in the right panel of Fig. 5. The predicted monopole flux limits will become weaker as the monopole velocity β increases. For comparison, we also show the Super-K published limit (dashed line) [18] in this figure. Note that it has been divided by a factor of 0.17 because of $\sigma_R = \sigma_0/\beta_{\text{rel}}^2$ used in Ref. [18] to describe the cross section of monopole-catalyzed proton decays, rather than $\sigma_R = 0.17\sigma_0/\beta_{\text{rel}}^2$ used in this paper. We find that the predicted and published limits have different behaviors for $\beta > 4.5 \times 10^{-3}$, which is caused by different results used for the capture fraction $\epsilon(M_M, \beta, g)$ in Eq. (2.2). As discussed in Sec. 2, $\epsilon(M_M, \beta, g)$ depends on the energy loss rate of monopoles passing through the Sun. The $\epsilon(M_M, \beta, g)$ calculation in Ref. [18] is based on the collective effects which can enhance the monopole energy loss rate [40]. Therefore, the Super-K has a limit on the monopole flux for $\beta > 4.5 \times 10^{-3}$ since these monopoles can be captured by the Sun due to the large stopping power. However, other calculations find that the energy loss from collective effects is insignificant [41, 42], and about one order smaller than that used in this paper [25]. So we do not consider the contribution from collective effects to the monopole stopping power. On the

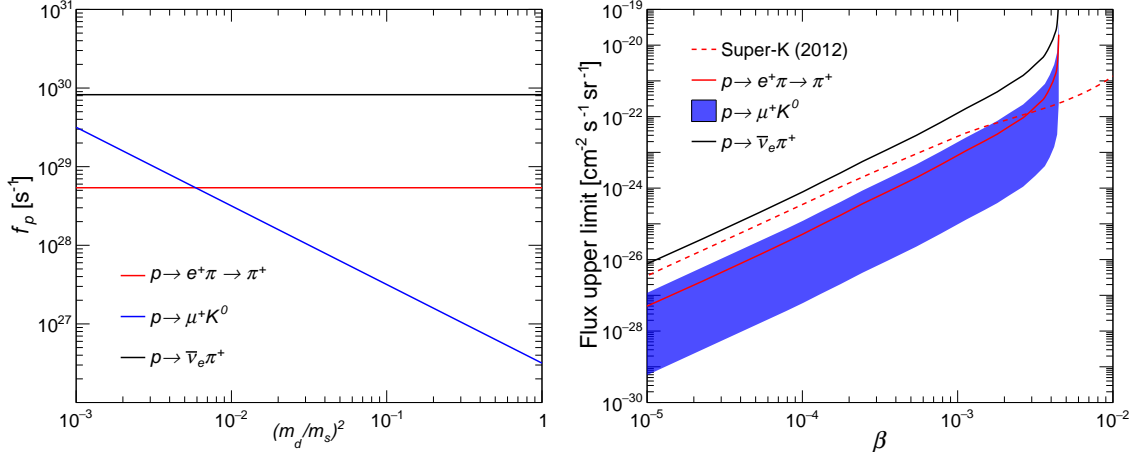


Figure 5. 90% C.L. upper limits to the monopole-catalyzed proton decay rate f_p (left panel) in the Sun and the monopole flux (right panel) for the Super-K 176 kton-year exposure. Here we take the branching ratios of $B(p \rightarrow e^+ \pi \rightarrow \pi^+) = 0.5$, $B(p \rightarrow \mu^+ K^0) \approx m_d^2/m_s^2$ and $B(p \rightarrow \bar{\nu}_e \pi^+) = 10^{-4}$. In the right figure, the catalysis cross section $\sigma_0 = 1$ mb, $M_M = 10^{16}$ GeV and the Dirac magnetic charge have been assumed for the GUT monopole, the blue band corresponds to m_d^2/m_s^2 in the range of $[1/400 - 1/2]$.

other hand, the predicted result (red line) is stronger than the published one (dashed line) if $\beta < 3 \times 10^{-3}$ for the proton decay mode $p \rightarrow e^+ \pi \rightarrow \pi^+$. This is because that we ignore the relevant uncertainties and use a different method to roughly calculate the sensitivity. Note that this difference does not change the conclusion that the proton decay mode $p \rightarrow \mu^+ K^0$ can give the best limit among the three decay modes for most of the parameter space.

6 Conclusions

In conclusion, we have investigated the neutrino signals from proton decays catalyzed by GUT monopoles in the Sun. Three typical proton decay modes, $p \rightarrow e^+ \pi$, $p \rightarrow \mu^+ K^0$ and $p \rightarrow \bar{\nu}_e \pi^+$, have been analyzed for the Super-K experiment. To obtain the neutrino energy spectra, we use the Geant4 software to simulate interactions of decay products in the highly-dense solar center. It is found that K^0 can produce a large amount of 236 MeV monoenergetic ν_μ neutrinos through the charge exchange process $K^0 + p \rightarrow K^+ + n$ and the subsequent decay $K^+ \rightarrow \mu^+ \nu_\mu$. This interesting feature is not realized in the previous papers. Based on the signal and background distributions of three proton decay modes, we set the reasonable selection conditions, and estimate the corresponding signal efficiencies and backgrounds in Super-K. Then we calculate the Super-K upper limit on the monopole-catalyzed proton decay rate f_p , and find $p \rightarrow \mu^+ K^0$ can give the best limit among three decay modes for most of the parameter space. Note that the decay mode $p \rightarrow \mu^+ K^0$ always give a better limit than $p \rightarrow \bar{\nu}_e \pi^+$. So we suggest the Super-K collaboration searches for this important proton decay mode in the future analysis. Finally, we present the Super-K sensitivities to the monopole flux for three proton decay modes.

Acknowledgments

This work is supported in part by the National Nature Science Foundation of China (NSFC) under Grants No. 11575201 and No. 11675273, and the Strategic Priority Research Program of the Chinese Academy of Sciences under Grant No. XDA10010100.

References

- [1] G. 't Hooft, Nucl. Phys. B **79** (1974), 276-284 doi:10.1016/0550-3213(74)90486-6
- [2] A. M. Polyakov, JETP Lett. **20** (1974), 194-195 PRINT-74-1566 (LANDAU-INST).
- [3] P. A. Zyla *et al.* [Particle Data Group], PTEP **2020** (2020) no.8, 083C01 doi:10.1093/ptep/ptaa104
- [4] S. Burdin, M. Fairbairn, P. Mermod, D. Milstead, J. Pinfold, T. Sloan and W. Taylor, Phys. Rept. **582** (2015), 1-52 doi:10.1016/j.physrep.2015.03.004 [arXiv:1410.1374 [hep-ph]].
- [5] L. Patrizii and M. Spurio, Ann. Rev. Nucl. Part. Sci. **65** (2015), 279-302 doi:10.1146/annurev-nucl-102014-022137 [arXiv:1510.07125 [hep-ex]].
- [6] N. E. Mavromatos and V. A. Mitsou, Int. J. Mod. Phys. A **35** (2020) no.23, 2030012 doi:10.1142/S0217751X20300124 [arXiv:2005.05100 [hep-ph]].
- [7] V. A. Rubakov, Nucl. Phys. B **203** (1982), 311-348 doi:10.1016/0550-3213(82)90034-7
- [8] C. G. Callan, Jr., Phys. Rev. D **26** (1982), 2058-2068 doi:10.1103/PhysRevD.26.2058
- [9] T. Kajita, K. Arisaka, M. Koshihara, M. Nakahata, Y. Oyama, A. Suzuki, M. Takita, Y. Totsuka, T. Kifune and T. Suda, *et al.* J. Phys. Soc. Jap. **54** (1985), 4065-4068 doi:10.1143/JPSJ.54.4065
- [10] J. E. Bartelt, H. Courant, K. J. Heller, T. Joyce, M. Marshak, E. Peterson, K. Ruddick, M. Shupe, D. S. Ayres and J. W. Dawson, *et al.* Phys. Rev. D **36** (1987), 1990 [erratum: Phys. Rev. D **40** (1989), 1701] doi:10.1103/PhysRevD.36.1990
- [11] R. Becker-Szendy, C. B. Bratton, J. Breault, D. Casper, S. T. Dye, K. Ganezer, W. Gajewski, M. Goldhaber, T. J. Haines and P. G. Halverson, *et al.* Phys. Rev. D **49** (1994), 2169-2173 doi:10.1103/PhysRevD.49.2169
- [12] V. A. Balkanov *et al.* [Baikal], Prog. Part. Nucl. Phys. **40** (1998), 391-401 doi:10.1016/S0146-6410(98)00047-7 [arXiv:astro-ph/9801044 [astro-ph]].
- [13] M. Ambrosio *et al.* [MACRO], Eur. Phys. J. C **26** (2002), 163-172 doi:10.1140/epjc/s2002-01045-x [arXiv:hep-ex/0207024 [hep-ex]].
- [14] M. G. Aartsen *et al.* [IceCube], Eur. Phys. J. C **74** (2014) no.7, 2938 [erratum: Eur. Phys. J. C **79** (2019) no.2, 124] doi:10.1140/epjc/s10052-014-2938-8 [arXiv:1402.3460 [astro-ph.CO]].
- [15] E. W. Kolb, S. A. Colgate and J. A. Harvey, Phys. Rev. Lett. **49** (1982), 1373 doi:10.1103/PhysRevLett.49.1373
- [16] K. Freese and E. Krasteva, Phys. Rev. D **59** (1999), 063007 doi:10.1103/PhysRevD.59.063007 [arXiv:astro-ph/9804148 [astro-ph]].
- [17] J. Arafune, M. Fukugita and S. Yanagita, Phys. Rev. D **32** (1985), 2586 doi:10.1103/PhysRevD.32.2586
- [18] K. Ueno *et al.* [Super-Kamiokande], Astropart. Phys. **36** (2012), 131-136 doi:10.1016/j.astropartphys.2012.05.008 [arXiv:1203.0940 [hep-ex]].
- [19] F. A. Bais, J. R. Ellis, D. V. Nanopoulos and K. A. Olive, Nucl. Phys. B **219** (1983), 189-219 doi:10.1016/0550-3213(83)90434-0

- [20] N. Houston, T. Li and C. Sun, JCAP **10** (2018), 034 doi:10.1088/1475-7516/2018/10/034 [arXiv:1803.02835 [hep-ph]].
- [21] T. W. B. Kibble, J. Phys. A **9** (1976), 1387-1398 doi:10.1088/0305-4470/9/8/029
- [22] E. N. Parker, Astrophys. J. **160** (1970), 383 doi:10.1086/150442
- [23] M. S. Turner, E. N. Parker and T. J. Bogdan, Phys. Rev. D **26** (1982), 1296 doi:10.1103/PhysRevD.26.1296
- [24] J. A. Frieman, K. Freese and M. S. Turner, Astrophys. J. **335** (1988), 844-861 doi:10.1086/166972
- [25] S. P. Ahlen, I. De Mitri, J. T. Hong and G. Tarle, Phys. Rev. D **55** (1997), 6584-6590 doi:10.1103/PhysRevD.55.6584
- [26] S. P. Ahlen, I. De Mitri, J. T. Hong and G. Tarle, INFN-AE-96-34.
- [27] J. Arafune and M. Fukugita, Phys. Rev. Lett. **50** (1983), 1901 doi:10.1103/PhysRevLett.50.1901
- [28] N. Vinyoles, A. M. Serenelli, F. L. Villante, S. Basu, J. Bergström, M. C. Gonzalez-Garcia, M. Maltoni, C. Peña-Garay and N. Song, Astrophys. J. **835** (2017) no.2, 202 doi:10.3847/1538-4357/835/2/202 [arXiv:1611.09867 [astro-ph.SR]].
- [29] J. Arafune and M. Fukugita, Phys. Lett. B **133** (1983), 380-384 doi:10.1016/0370-2693(83)90810-9
- [30] P. Baratella, M. Cirelli, A. Hektor, J. Pata, M. Piibeleht and A. Strumia, JCAP **03** (2014), 053 doi:10.1088/1475-7516/2014/03/053 [arXiv:1312.6408 [hep-ph]].
- [31] S. Agostinelli *et al.* [GEANT4], Nucl. Instrum. Meth. A **506** (2003), 250-303 doi:10.1016/S0168-9002(03)01368-8
- [32] T. T. Böhlen, F. Cerutti, M. P. W. Chin, A. Fassò, A. Ferrari, P. G. Ortega, A. Mairani, P. R. Sala, G. Smirnov and V. Vlachoudis, Nucl. Data Sheets **120** (2014), 211-214 doi:10.1016/j.nds.2014.07.049
- [33] W. L. Guo, Phys. Rev. D **99** (2019) no.7, 073007 doi:10.1103/PhysRevD.99.073007 [arXiv:1812.04378 [hep-ph]].
- [34] A. Strumia and F. Vissani, Phys. Lett. B **564** (2003), 42-54 doi:10.1016/S0370-2693(03)00616-6 [arXiv:astro-ph/0302055 [astro-ph]].
- [35] C. Andreopoulos, A. Bell, D. Bhattacharya, F. Cavanna, J. Dobson, S. Dytman, H. Gallagher, P. Guzowski, R. Hatcher and P. Kehayias, *et al.* Nucl. Instrum. Meth. A **614** (2010), 87-104 doi:10.1016/j.nima.2009.12.009 [arXiv:0905.2517 [hep-ph]].
- [36] Y. Ashie *et al.* [Super-Kamiokande], Phys. Rev. D **71** (2005), 112005 doi:10.1103/PhysRevD.71.112005 [arXiv:hep-ex/0501064 [hep-ex]].
- [37] V. Takhistov *et al.* [Super-Kamiokande], Phys. Rev. Lett. **113** (2014) no.10, 101801 doi:10.1103/PhysRevLett.113.101801 [arXiv:1409.1947 [hep-ex]].
- [38] T. Tanaka *et al.* [Super-Kamiokande], Astrophys. J. **742** (2011), 78 doi:10.1088/0004-637X/742/2/78 [arXiv:1108.3384 [astro-ph.HE]].
- [39] W. L. Guo, JCAP **01** (2016), 039 doi:10.1088/1475-7516/2016/01/039 [arXiv:1511.04888 [hep-ph]].
- [40] A. J. S. Hamilton and C. L. Sarazin, Astrophys. J. **274** (1983), 399-407 doi:10.1086/161455
- [41] N. Meyer-Vernet, Astrophys. J. **290** (1985), 21-23 doi:10.1086/162954
- [42] L. Bracci, G. Fiorentini and G. Mezzorani, Nucl. Phys. B **258** (1985), 726-746 doi:10.1016/0550-3213(85)90633-9